

Solvent Annealing of Striped Ellipsoidal Block Copolymer Particles: Reversible Control over Lamellae Asymmetry, Aspect Ratio, and Particle Surface

Lucila Navarro, Andreas F. Thünemann, and Daniel Klinger*

Cite This: *ACS Macro Lett.* 2022, 11, 329–335

Read Online

ACCESS |



Metrics & More

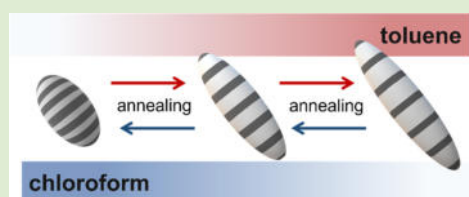


Article Recommendations



Supporting Information

ABSTRACT: Solvent annealing is a versatile tool to adjust the shape and morphology of block copolymer (BCP) particles. During this process, polar solvents are often used for block-selective swelling. However, such water-miscible solvents can induce (partial) solubilization of one block in the surrounding aqueous medium, thus, causing complex structural variations and even particle disassembly. To reduce the complexity in morphology control, we focused on toluene as a nonpolar polystyrene-selective solvent for the annealing of striped polystyrene-*b*-poly(2-vinylpyridine) (PS-*b*-P2VP) ellipsoids. The selective stretching of PS chains produces unique asymmetric lamellae structures, which translate to an increase in the particle aspect ratio after toluene evaporation. Complete reversibility is achieved by changing to chloroform as a nonselective solvent. Moreover, surfactants can be used to tune block-selective wetting of the particle surface during the annealing; for example, a PS shell can protect the internal lamellae structure from disassembly. Overall, this versatile postassembly process enables the tailoring of the structural features of striped colloidal ellipsoids by only using commercial BCPs and solvents.



Shape anisotropic particles with defined internal nanostructures are promising building blocks for advanced applications in biology, photonics, catalysis, and so on.^{1–4} To prepare such multifunctional colloids, evaporation-induced self-assembly of block copolymers (BCPs) has been established as a versatile method.⁵ While the BCP volume ratio (packing parameter) determines the general morphology, the soft confinement of the emulsion droplets allows further structural variations. For this, various parameters can be adjusted during phase separation: the interfacial energies between BCP and the surrounding medium, the degree of confinement, the evaporation temperature, the pH of the continuous phase, and the evaporation kinetics.^{6–11} In addition, the incorporation or removal of additives,¹² for example, different solvents,¹³ small molecules,^{14,15} homopolymers,^{7,16,17} and even other (block) copolymers,^{18,19} enable complex structures during particle preparation that can deviate from the pure BCP systems.

Alternatively, postassembly treatments allow adjusting shape and morphology of BCP particles after their preparation.^{20–23} Among such strategies, (vapor) solvent annealing is a versatile residue-free method that is well-established for BCP thin films^{24–27} but is still in its infancy for BCP particles. Here, current investigations often focus on controlling the domain orientation for a given underlying morphology. In colloidal systems, this can be achieved through varying the surfactants at the BCP/water interface.^{20,21,28} For example, in particles with a lamellar morphology, a light-induced reversible shift between concentric-lamellar spheres and striped lamellar ellipsoids can be achieved by UV-responsive surfactants.^{29,30} For such domain

reorientations, a nonselective solvent is required to enable high mobility of both blocks without changing the BCP packing parameter during the annealing process.

In contrast, the utilization of block-selective solvents can actually change the underlying morphology by tuning the solubility and associated stretching of the individual BCP segments. The resulting variation of the BCP packing parameter induces a morphological transformation. This process strongly depends on the polarity and miscibility of the annealing solvent with the surrounding phase. In water, polar block-selective solvents can lead to a high swelling or even (partial) solubilization of one block, thus, causing structural variations and even disassembly.^{31–33} For example, spherical polystyrene-*b*-poly(2-vinyl pyridine) (PS-*b*-P2VP) particles with concentric lamellae can transfer into vesicular structures upon the addition of ethanol as a highly polar P2VP-selective solvent.²² Contrarily, nonpolar block selective solvents are less explored. Such water immiscible solvents selectively induce chain stretching in the respective domains. In combination with the less flexible nonswollen domains that can act as physical boundaries, complex morphological transformations can be induced. However, more investigations are needed to determine

Received: October 26, 2021

Accepted: February 8, 2022

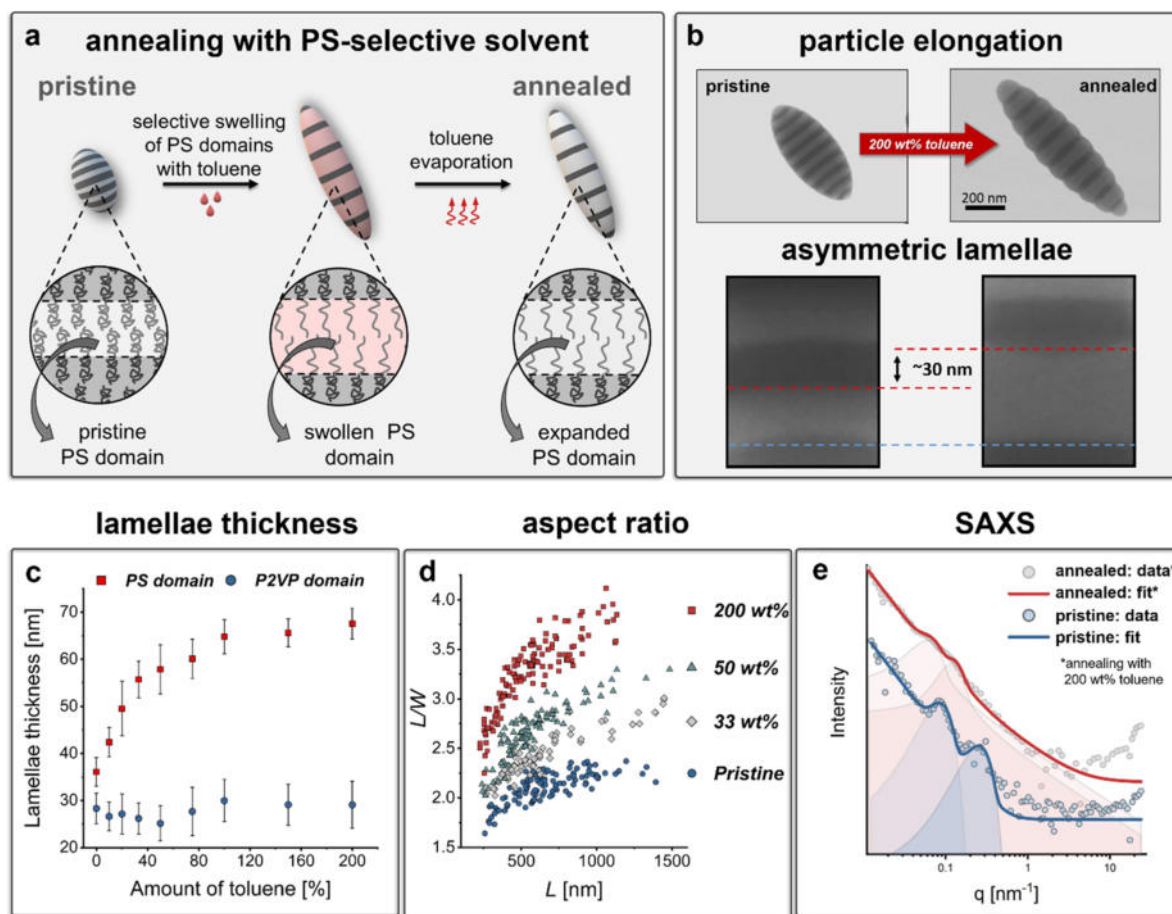


Figure 1. (a) Schematic representation of the particle solvent annealing process: Toluene as a selective solvent for the PS segments is added to a suspension of pristine PS-*b*-P2VP particles. The resulting stretching of the PS selectively increases the PS lamellae thickness and translates to particle elongation after solvent evaporation. (b) Comparing TEM images of pristine and annealed particles shows a particle elongation, that is, an increase in the aspect ratio for the same number of 10 lamellae per particle. The detailed pictures of the particles' middle sections show an exclusive increment of approximately 30 nm in the PS thickness, thus, resulting in an asymmetric lamellae morphology. (c) While PS lamellae thickness increases with the amount of toluene in the annealing process, the P2VP lamellae thickness remains unchanged. (d) The aspect ratio of annealed particles increases with toluene (e.g., 33, 50, and 200 wt %) and depends on the particles' long axis, that is, the number of lamellae per particle. (e) Small angle X-ray scattering patterns of pristine and annealed particles (200 wt % of toluene) show an increase in domain spacing after annealing.

the potential of such strategies for tailoring BCP particle shape and morphology.

In addressing this need, we aim to investigate such phenomena in striped ellipsoidal particles. In such stacked lamellar structures, chain stretching can occur almost freely in the *z*-direction (perpendicular to the lamellae), that is, the influence of the nonswollen domains is minimized. Thus, selective swelling of one domain can translate to a particle elongation, that is, a change in aspect ratio while maintaining the lamellar morphology. While this is reported for cross-linked domains (via the addition of organic solvents³⁴ or pH changes⁶), the cross-linking points prevent the retention of chain stretching after solvent evaporation. Thus, the initial structure (as before "annealing") is restored in these cases. In un-cross-linked domains, it is assumed that this process is different. Here, the chains can remain stretched after solvent evaporation. However, since chain stretching is entropically unfavored, this either requires kinetic trapping or enthalpic compensation. In such cases, we hypothesize that the final annealed structure consists of asymmetric lamellae, that is, different BCP domains with different thicknesses (see Figure 1a). Targeting such asymmetric structures through established assembly methods would require complex miktoarm star copolymer architectures that are difficult

to synthesize.³⁵ In contrast our suggested postassembly method is based on easily accessible commercial linear diblock copolymers and common solvents. Thus, this strategy would represent a facile and robust alternative to tailoring the aspect ratio and lamellar thickness of such colloidal ellipsoids.

To examine the effect of a selective nonpolar solvent on the morphology of lamellar BCP particles, we used striped PS-*b*-P2VP ellipsoids and toluene as a PS-selective solvent. The particles were prepared according to our previously published method that uses a mixed surfactant system to provide neutral wetting conditions for both blocks at the interphase.⁶ After particle preparation, different amounts of toluene were directly added (via micropipette) to the dispersion of striped ellipsoids. By avoiding the uncontrolled transfer of the solvent from a vapor phase to the dispersion (as reported for vapor annealing processes), the toluene amount could be controlled precisely. After solvent addition, the mixtures were briefly sonicated to generate small droplets of toluene, thus, enhancing the solvent's surface to volume ratio and enable fast diffusion into the particles. Toluene amounts were gradually varied between 10 and 250 wt % with respect to the total mass of pristine particles. After a predetermined time for swelling, toluene was evaporated to obtain solid non-swollen particles.

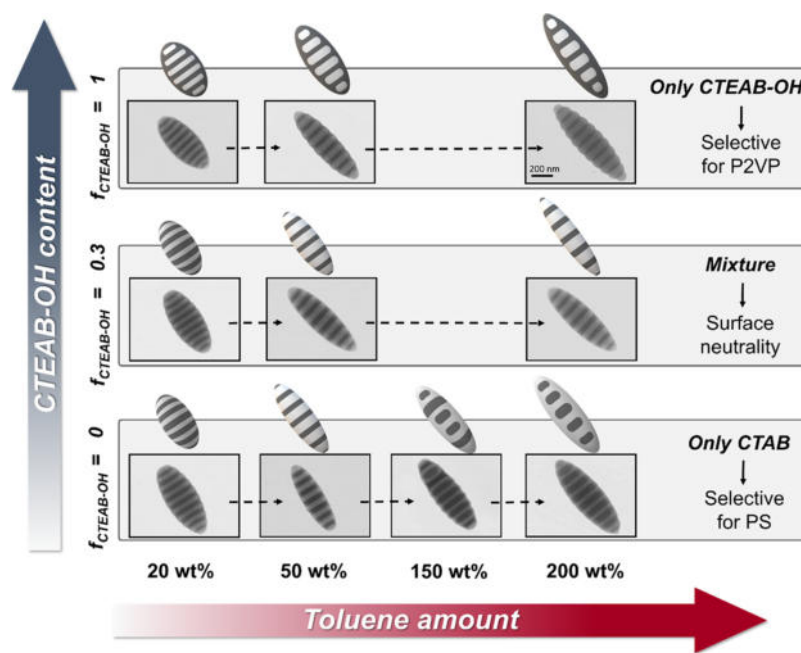


Figure 2. Influence of surfactants on the particle morphology after annealing with different amounts of toluene. By varying the composition of a surfactant mixture consisting of PS-selective CTAB and P2VP-selective CTEAB-OH, the wetting of the particle surface by the different BCP segments can be controlled. This depends on the amount of toluene, as the solvent is assumed to act as a plasticizer for the P2VP domains. Thus, high toluene contents above 150 wt % can induce a full P2VP (for pure CTEAB-OH) or PS (for pure CTAB) shell around the particles. A surfactant mixture with a CTEAB-OH content of 0.3 can ensure neutral wetting of the BC/water interface.

For increasing toluene content, transmission electron microscopy (TEM) revealed an exclusive increase of the PS domain thickness. This translates to an increase in aspect ratio ($AR = L/W$), that is, particle elongation (Figures 1, S1, and S2). The underlying process involves the selective expansion of the PS chains (due to their toluene affinity) and retention of the stretched conformation after evaporation (see Figure 1a). For annealing with 200 wt % of toluene, this phenomenon is most prominent and the PS lamellae thickness increased from 36 ± 5 nm (before annealing) to 67 ± 5 nm (after annealing; Figure 1b). Depending on the number of PS lamellae per particle, this can almost double the aspect ratio (Figure 1d). For example, a 1.7-fold increase from $AR = 2.2$ to 3.7 is observed for particles with 10 PS domains (Figure 1b). Since the P2VP domain thickness remains constant during this process (see Figures 1c and S1), the aspect ratio increment corresponds to a new asymmetric lamellar morphology with PS domains being thicker than P2VP domains.

The asymmetry of morphology and shape can be tuned precisely by varying the amount of toluene. Figure 1c shows a steep increase in PS domain thickness for toluene contents up to 100 wt %. For additional toluene amounts, a plateau is reached at a PS thickness of around 62–67 nm. In contrast, the thickness of the P2VP domains remains similar to the pristine particles. While these values were obtained from TEM analysis, we also aimed to evaluate the increase of lamellar domain spacing more quantitatively. For this, SAXS measurements were performed on pristine and highly swollen particles with 200 wt % of toluene (Figures 1e and S3). For pristine particles, the peak maxima are observed at $q_1 = 0.08 \text{ nm}^{-1}$ and $q_2 = 0.252 \text{ nm}^{-1}$ (indexed as (001) and (003) since $q_2 = 3q_1$). This translates to a domain spacing of $d = 2\pi/q_1 = d_{PS} + d_{P2VP}$ of 75 nm. In contrast, for the swollen particles, the peak maxima are observed at $q_1 = 0.06 \text{ nm}^{-1}$ and $q_2 = 0.12 \text{ nm}^{-1}$ (indexed as (001) and (002) since $q_2 =$

$2q_1$). Thus, the domain spacing for the swollen particles was 100 nm. Assuming that the P2VP thickness remains constant (as seen in TEM), the 25 nm increment can be attributed to an exclusive increase of PS thickness. This enlarged domain spacing from SAXS (+25 nm) correlates well with the value obtained from TEM (+30 nm), and slight differences are attributed to the error of manual measurements in TEM ($d_{\text{pristine}} = 66 \pm 5$ nm and $d_{\text{swollen}} = 95 \pm 7$ nm).

The increase of PS domain thickness increases the particle length (L). Since the width (W) remains constant, particle AR increases with toluene content (Figures 1d and S4). However, AR also varies with particle size, described by length (L). This correlation is already observed in the preparation of pristine particles and results from the thermodynamics of the BCP phase separation. Since surface energy influences ellipsoid formation, larger particles are easier to deform due to their lower surface to volume ratio.⁶ As shown in Figure 1d, this trend is transferred to the annealed particles. For 33, 50, and 200 wt % toluene, the AR increases with L for each sample. Moreover, the AR difference between annealed and pristine particles is more pronounced for larger particles (for all samples see Figure S5).

Overall, this postassembly strategy is simple, robust, and mainly depends on the amount of toluene. To confirm this, we carefully screened the influence of other parameters, such as swelling temperature (Figure S6), swelling time (Figure S7), and toluene evaporation rate (Figure S8). These tests did not reveal any additional effect (see Table S2). Thus, aspect ratios up to $AR = 4$ and asymmetric morphologies with PS domains being double as thick as P2VP domains can be achieved by simply varying the toluene content between 0 and 200 wt %. However, exceeding 200 wt % can lead to a loss of the lamellar morphology. As shown in Figure S9, a complete rearrangement of the particles to a spherical shape with multiple P2VP centers is observed for toluene amounts of 250 wt %. This is assumed to be

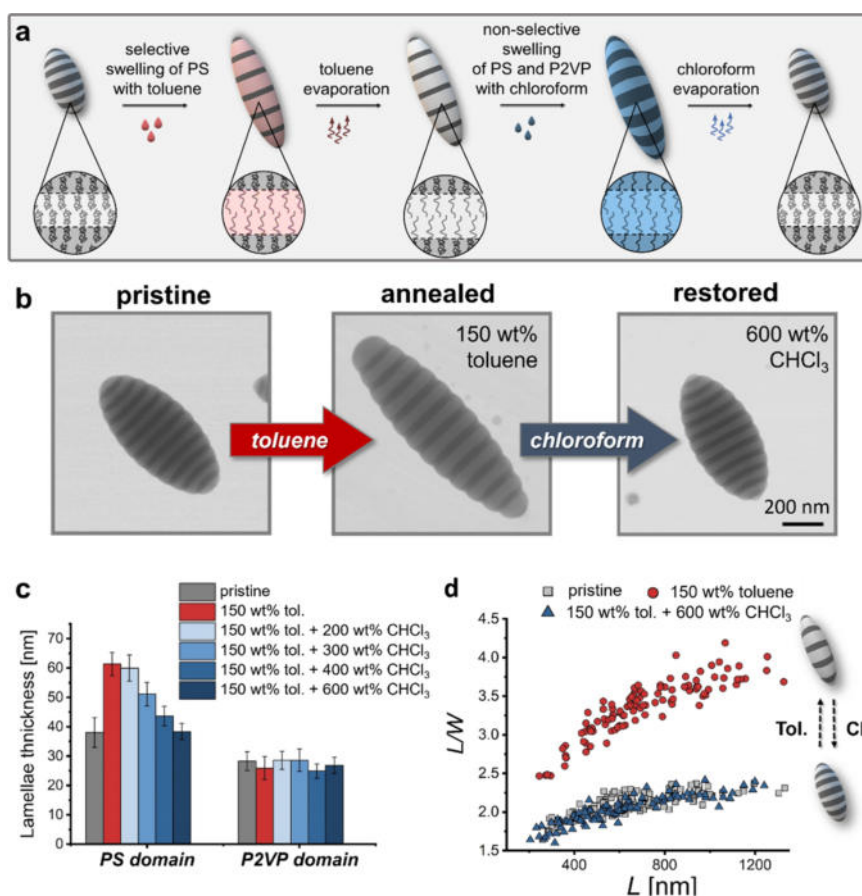


Figure 3. (a) Schematic representation showing the reversibility of the annealing process. An initial solvent annealing step with toluene as block-selective solvent will mainly expand the PS domains after evaporation. Subsequent swelling with chloroform, as a nonselective solvent for both domains, will equally mobilize both blocks and restore the initial particle shape and morphology after evaporation. (b) TEM pictures of particles at different stages of the process demonstrate the reversibility. Starting from pristine particles, PS-selective annealing with 150 wt % of toluene (at $f_{\text{CTEAB-OH}} = 0.7$) leads to elongated particles with an increased thickness of PS domains. The initial structure can be restored by subsequent annealing with 600 wt % of chloroform. (c) PS and P2VP lamellae thicknesses for different amounts of chloroform show that restoration of the initial domain sizes requires at least 600 wt % of chloroform. (d) For elongated particles that were annealed with 150 wt % of toluene, the aspect ratio distribution of pristine particles can be completely restored by the subsequent annealing with 600 wt % of chloroform.

the result of P2VP plasticization by such large amounts of toluene.³⁶

While this method allows accurate control over asymmetric lamellae morphologies, interpretation of the underlying annealing process is challenging. Overall, the entropically unfavored stretching of PS chains requires kinetic stabilization or energetic compensation. While fast vitrification of swollen domains could trap such energetically unfavored structures, the influence of evaporation rate on the morphology is negligible (Figure S8). Hence, we suggest enthalpic compensation due to structural changes at the BCP/water interface. Examining annealed particles in more detail, a thin layer of P2VP was observed to cover the particle surface (Figure S10). This suggests P2VP plasticization to allow partial migration of P2VP segments to the BCP/water interface. The preferential affinity of P2VP for the aqueous phase shows a disturbed balance of the neutral wetting conditions that are initially defined during preparation of the pristine particles.³⁷ Originally, a mixture of PS- and P2VP-selective surfactants (CTAB and CTEAB-OH, respectively) was carefully adjusted to the BCP volume ratio. However, during annealing, the PS domains expand and the corresponding surface area increases, that is, about +30% for annealing with 150 wt % toluene (see Figure S11). As a result, domain sizes do not match the initial surfactant ratio anymore,

and the increased PS/water interface is energetically unfavored. We assume this effect is mediated by BCP rearrangements at the particle surface to cover the PS domains with P2VP. Since this reduces the PS/water interface, the corresponding enthalpic gain compensates for the entropically unfavored PS stretching.

These results suggest stabilization of the asymmetric lamellae through the BCP/water interface. Since this interface is governed by the surfactants, varying the surfactant ratio should enable further tuning of the final morphology. To investigate this influence, the pristine particles were first purified by cycles of centrifugation and redispersion in different surfactant mixtures before annealing with toluene. Figure 2 shows the variety of structures obtained for different contents of CTEAB-OH, denoted as the weight fraction $f_{\text{CTEAB-OH}}$. An overview of the conditions is shown in Table S3, and additional TEM images are shown in Figures S12 and S13. In these experiments, a surfactant mixture with $f_{\text{CTEAB-OH}} = 0.3$ provided neutral wetting of both blocks at the particle surface. Here, we assume that the excess of PS-selective CTAB (70 wt %) can stabilize the additional PS/water interface. Since no redistribution of P2VP occurs, the P2VP chains can also stretch and the lamellar asymmetry ($d_{\text{PS}}/d_{\text{P2VP}}$) is reduced (Figures S14 and S15). Simultaneous reduction of PS expansion suggests that stabilization of the PS surface with CTAB is less effective than by P2VP migration.

These assumptions are further supported by control experiments using CTEAB-OH contents of $f_{\text{CTEAB-OH}} = 0.65$ and 0.75 (close to the initial composition $f_{\text{CTEAB-OH}} = 0.70$; Figures S10 and S13). Here, P2VP domains preferably interact with the excess CTEAB-OH, leading to partial engulfing of the PS domains. This P2VP redistribution then increases the lamellae asymmetry again (see Figures S14 and S15). Overall, these findings suggest that the additional PS surface can be stabilized either directly by using more PS-selective CTAB or indirectly by a partial migration of P2VP segments to engulf the PS domains and minimize the PS/water interface. In both cases, it is assumed that these favorable interactions can compensate the entropically unfavored stretching of the PS chains.

In addition to these mechanistic considerations, varying the surfactants also allows further tuning of the particle structure via annealing. It is assumed that a complete wetting of one block can be induced by resuspending the particles in a single surfactant solution. Indeed, by using a mass fraction of $f_{\text{CTEAB-OH}}$ of 1 (only CTEAB-OH) migration of P2VP to the particle surface is observed for all toluene amounts. As discussed above, this contributes to a large lamellar asymmetry (Figure S14). In contrast, a mass fraction of $f_{\text{CTEAB-OH}}$ of 0 (only CTAB, selective for PS) induced migration of PS to the particle surface. This process depends on the amount of toluene and the corresponding level of PS chain mobility. A total of 20 to 50 wt % of toluene is not enough to induce complete PS migration to the interface. Instead, both domains are wetting the interface equally. Increasing the toluene amount to 150 wt %, morphological changes become obvious. In an intermediate state, part of the PS is able to migrate to the interface, while still some P2VP lamellae are exposed to the surface. For 200 wt % of toluene, this transition is complete and particles are obtained that are fully covered with a PS layer. Interestingly, this PS migration can stabilize a certain extent of P2VP chain stretching to cause an inverted lamellar asymmetry $d_{\text{P2VP}} > d_{\text{PS}}$. These results deviate from established annealing processes with a non-selective “good” solvent for both blocks. In such cases, a preferential interaction of one block with the surrounding surfactants will result in onion-like particles. In contrast, the utilization of toluene as block-selective nonpolar solvent restricts the chain motion of both blocks. This only allows the migration of a single domain to the particle interface and keeps the striped ellipsoidal shape.

Such new morphologies exhibit a homogeneous particle surface chemistry, which governs their behavior in dispersion. For example, a surrounding PS layer provides structural stabilization of the lamellar morphology against disassembly. As shown for striped PS-*b*-P2VP particles, low pH values can protonate the P2VP blocks, thus, inducing their water solubility. As a result, the particles disassemble into PS discs with dangling P2VP chains. Now this effect can be controlled by changing the structure of the particles through a quick annealing step. To evaluate this approach, annealed particles with different morphologies were acidified to pH 2–3 and their structure was determined by TEM (Figure S16). For particles with a surrounding P2VP shell (annealed in the presence of CTEAB-OH), a low pH induced complete disassembly into discrete PS disks. In contrast, a PS surface (annealed in the presence of CTAB) prevents the disassembly. For intermediate morphologies (annealed in the presence of CTAB and CTEAB-OH mixtures), disassembly occurs on the P2VP lamellae facing the aqueous phase. Thus, varying the surfactants during the

annealing process enhances the portfolio of simple methods that can be used to control the particle properties in dispersion.

Since toluene annealing is a physical process to induce spatial and conformational changes in the BCP chains, it should be reversible. Thus, an equal mobilization of both blocks under neutral wetting conditions should restore the initial shape and morphology upon solvent evaporation. For this, a good solvent for both blocks is required. To test this assumption, pristine particles were first annealed with 150 wt % of toluene to induce particle elongation upon stretching of the PS domains. Then, chloroform was added as a “good” solvent in different amounts and slowly evaporated (see Figure 3a). By examining the particle structures after the second annealing step, it was found that chloroform is able to induce morphological changes that are concentration-dependent. As shown by TEM images in Figure 3b, the particles' initial structure (AR and domain thickness) was completely restored for 600 wt % of chloroform (also see Figures S17 and S18). Between 200 and 600 wt % of added chloroform, the PS lamella thickness (Figure 3c) and the particle aspect ratio (Figures 3d and S13b) are progressively returning to their original values. These observations support our hypothesis of the underlying process and provide additional versatility to tune the particles' structure.

In summary, we have demonstrated a new postassembly strategy to control the shape and morphology of striped PS-*b*-P2VP ellipsoids. The block-selective solvent annealing process gives access to unique asymmetric domain structures and allows accurate control over four parameters: PS lamellar thickness, particle aspect ratio, domain orientation at the BCP/water interphase, and reversibility. A key benefit of this process is the ability to gradually change the particles' structural features by solely adjusting the amount of solvent. This highlights the simplicity and the robustness of this process. Using toluene as a PS-selective nonpolar solvent enables asymmetric lamellae with the PS domains being roughly double the size as the P2VP domains. This translates into particle elongation and an increase of aspect ratio. Depending on the number of lamellae per particle, AR can almost double to values of almost 4. In addition, the domain orientation at the particle surface can be controlled through the surfactants. This enables to select a single domain to cover the entire particle surface and protect the internal lamellar structure from disassembly. Finally, complete reversibility is achieved by changing the annealing solvent to a nonselective solvent. Overall, the process represents a new synthetic tool to access a variety of new structures from a single batch of preformed particles.

■ ASSOCIATED CONTENT

SI Supporting Information

The Supporting Information is available free of charge at <https://pubs.acs.org/doi/10.1021/acsmacrolett.1c00665>.

Description of materials, synthetic procedures, and characterization methods. Small-angle X-ray scattering (SAXS): experimental procedure, peak fitting, and data processing. Experimental procedure for particle synthesis and annealing. Supporting figures: TEM images for annealed particles, SAXS patterns with all fits, analysis of particle shape (length, width, aspect ratio), influence of annealing conditions (temperature, time, evaporation rate), particle surface areas and lamellar asymmetry, reversibility of annealing (PDF)

AUTHOR INFORMATION

Corresponding Author

Daniel Klinger – Institute of Pharmacy (Pharmaceutical Chemistry), Freie Universität Berlin, 14195 Berlin, Germany; orcid.org/0000-0002-8876-5088; Email: daniel.klinger@fu-berlin.de

Authors

Lucila Navarro – Institute of Pharmacy (Pharmaceutical Chemistry), Freie Universität Berlin, 14195 Berlin, Germany
Andreas F. Thünemann – Bundesanstalt für Materialforschung und -prüfung (BAM), 12205 Berlin, Germany; orcid.org/0000-0002-9883-6134

Complete contact information is available at:

<https://pubs.acs.org/10.1021/acsmacrolett.1c00665>

Notes

The authors declare no competing financial interest.

ACKNOWLEDGMENTS

The authors would like to thank Glen J. Smales for the help in SAXS measurements. L.N. acknowledges the funding from the European Union's Horizon 2020 research and innovation programme under the Marie Skłodowska-Curie Grant agreement No. 838448. We would like to acknowledge the assistance of the Core Facility BioSupraMol supported by the DFG.

REFERENCES

- (1) Shin, J. J.; Kim, E. J.; Ku, K. H.; Lee, Y. J.; Hawker, C. J.; Kim, B. J. 100th Anniversary of Macromolecular Science Viewpoint: Block Copolymer Particles: Tuning Shape, Interfaces, and Morphology. *ACS Macro Lett.* **2020**, *9* (3), 306–317.
- (2) Chen, C.; Wylie, R. A. L.; Klinger, D.; Connal, L. A. Shape Control of Soft Nanoparticles and Their Assemblies. *Chem. Mater.* **2017**, *29* (5), 1918–1945.
- (3) He, Q.; Ku, K. H.; Vijayamohan, H.; Kim, B. J.; Swager, T. M. Switchable Full-Color Reflective Photonic Ellipsoidal Particles. *J. Am. Chem. Soc.* **2020**, *142* (23), 10424–10430.
- (4) Varadharajan, D.; Turgut, H.; Lahann, J.; Yabu, H.; Delaittre, G. Surface-Reactive Patchy Nanoparticles and Nanodiscs Prepared by Tandem Nanoprecipitation and Internal Phase Separation. *Adv. Funct. Mater.* **2018**, *28* (39), 1800846.
- (5) Ku, K. H.; Shin, J. M.; Yun, H.; Yi, G.-R.; Jang, S. G.; Kim, B. J. Multidimensional Design of Anisotropic Polymer Particles from Solvent-Evaporative Emulsion. *Adv. Funct. Mater.* **2018**, *28* (42), 1802961.
- (6) Klinger, D.; Wang, C. X.; Connal, L. A.; Audus, D. J.; Jang, S. G.; Kraemer, S.; Killops, K. L.; Fredrickson, G. H.; Kramer, E. J.; Hawker, C. J. A Facile Synthesis of Dynamic, Shape-Changing Polymer Particles. *Angew. Chem., Int. Ed.* **2014**, *53* (27), 7018–7022.
- (7) Jeon, S.-J.; Yi, G.-R.; Yang, S.-M. Cooperative Assembly of Block Copolymers with Deformable Interfaces: Toward Nanostructured Particles. *Adv. Mater.* **2008**, *20* (21), 4103–4108.
- (8) Steinhaus, A.; Pelras, T.; Chakraborty, R.; Gröschel, A. H.; Müllner, M. Self-Assembly of Diblock Molecular Polymer Brushes in the Spherical Confinement of Nanoemulsion Droplets. *Macromol. Rapid Commun.* **2018**, *39* (19), 1800177.
- (9) Yabu, H.; Higuchi, T.; Shimomura, M. Unique Phase-Separation Structures of Block-Copolymer Nanoparticles. *Adv. Mater.* **2005**, *17* (17), 2062–2065.
- (10) Shin, J. M.; Kim, Y.; Yun, H.; Yi, G.-R.; Kim, B. J. Morphological Evolution of Block Copolymer Particles: Effect of Solvent Evaporation Rate on Particle Shape and Morphology. *ACS Nano* **2017**, *11* (2), 2133–2142.
- (11) Lee, J.; Ku, K. H.; Park, C. H.; Lee, Y. J.; Yun, H.; Kim, B. J. Shape and Color Switchable Block Copolymer Particles by Temperature and pH Dual Responses. *ACS Nano* **2019**, *13* (4), 4230–4237.
- (12) Xu, J.; Yang, Y.; Wang, K.; Li, J.; Zhou, H.; Xie, X.; Zhu, J. Additives Induced Structural Transformation of ABC Triblock Copolymer Particles. *Langmuir* **2015**, *31* (40), 10975–10982.
- (13) Deng, R.; Zheng, L.; Mao, X.; Li, B.; Zhu, J. Transformable Colloidal Polymer Particles with Ordered Internal Structures. *Small* **2021**, *17* (4), 2006132.
- (14) Lee, S.; Shin, J. J.; Ku, K. H.; Lee, Y. J.; Jang, S. G.; Yun, H.; Kim, B. J. Interfacial Instability-Driven Morphological Transition of Prolate Block Copolymer Particles: Striped Football, Larva to Sphere. *Macromolecules* **2020**, *53* (16), 7198–7206.
- (15) Klinger, D.; Robb, M. J.; Spruell, J. M.; Lynd, N. A.; Hawker, C. J.; Connal, L. A. Supramolecular guests in solvent driven block copolymer assembly: from internally structured nanoparticles to micelles. *Polym. Chem.* **2013**, *4* (19), 5038–5042.
- (16) Schmidt, B. V. K. J.; Elbert, J.; Scheid, D.; Hawker, C. J.; Klinger, D.; Gallei, M. Metallopolymer-Based Shape Anisotropic Nanoparticles. *ACS Macro Lett.* **2015**, *4* (7), 731–735.
- (17) Okubo, M.; Saito, N.; Takekoshi, R.; Kobayashi, H. Morphology of polystyrene/polystyrene-block-poly(methyl methacrylate)/poly(methyl methacrylate) composite particles. *Polymer* **2005**, *46* (4), 1151–1156.
- (18) Grundy, L. S.; Lee, V. E.; Li, N.; Sosa, C.; Mulhearn, W. D.; Liu, R.; Register, R. A.; Nikoubashman, A.; Prud'homme, R. K.; Panagiotopoulos, A. Z.; Priestley, R. D. Rapid Production of Internally Structured Colloids by Flash Nanoprecipitation of Block Copolymer Blends. *ACS Nano* **2018**, *12* (5), 4660–4668.
- (19) Kim, E. J.; Shin, J. M.; Kim, Y.; Ku, K. H.; Yun, H.; Kim, B. J. Shape control of nanostructured cone-shaped particles by tuning the blend morphology of A-b-B diblock copolymers and C-type copolymers within emulsion droplets. *Polym. Chem.* **2019**, *10* (19), 2415–2423.
- (20) Deng, R.; Liang, F.; Li, W.; Yang, Z.; Zhu, J. Reversible Transformation of Nanostructured Polymer Particles. *Macromolecules* **2013**, *46* (17), 7012–7017.
- (21) Shin, J. M.; Lee, Y. J.; Kim, M.; Ku, K. H.; Lee, J.; Kim, Y.; Yun, H.; Liao, K.; Hawker, C. J.; Kim, B. J. Development of Shape-Tuned, Monodisperse Block Copolymer Particles through Solvent-Mediated Particle Restructuring. *Chem. Mater.* **2019**, *31* (3), 1066–1074.
- (22) Fan, H.; Jin, Z. Selective Swelling of Block Copolymer Nanoparticles: Size, Nanostructure, and Composition. *Macromolecules* **2014**, *47* (8), 2674–2681.
- (23) Mei, S.; Jin, Z. Mesoporous Block-Copolymer Nanospheres Prepared by Selective Swelling. *Small* **2013**, *9* (2), 322–329.
- (24) Son, J. G.; Gotrik, K. W.; Ross, C. A. High-Aspect-Ratio Perpendicular Orientation of PS-b-PDMS Thin Films under Solvent Annealing. *ACS Macro Lett.* **2012**, *1* (11), 1279–1284.
- (25) Sinturel, C.; Vayer, M.; Morris, M.; Hillmyer, M. A. Solvent Vapor Annealing of Block Polymer Thin Films. *Macromolecules* **2013**, *46* (14), 5399–5415.
- (26) Baruth, A.; Seo, M.; Lin, C. H.; Walster, K.; Shankar, A.; Hillmyer, M. A.; Leighton, C. Optimization of Long-Range Order in Solvent Vapor Annealed Poly(styrene)-block-poly(lactide) Thin Films for Nanolithography. *ACS Appl. Mater. Interfaces* **2014**, *6* (16), 13770–13781.
- (27) Montarnal, D.; Delbosco, N.; Chamignon, C.; Violeaud, M.-A.; Luo, Y.; Hawker, C. J.; Drockenmüller, E.; Bernard, J. Highly Ordered Nanoporous Films from Supramolecular Diblock Copolymers with Hydrogen-Bonding Junctions. *Angew. Chem., Int. Ed.* **2015**, *54* (38), 11117–11121.
- (28) Qiang, X.; Dai, X.; Steinhaus, A.; Gröschel, A. H. Multicompartment Microparticles with Patchy Topography through Solvent-Adsorption Annealing. *ACS Macro Lett.* **2019**, *8* (12), 1654–1659.
- (29) Lee, J.; Ku, K. H.; Kim, M.; Shin, J. M.; Han, J.; Park, C. H.; Yi, G.-R.; Jang, S. G.; Kim, B. J. Stimuli-Responsive, Shape-Transforming Nanostructured Particles. *Adv. Mater.* **2017**, *29* (29), 1700608.

(30) Lee, J.; Ku, K. H.; Kim, J.; Lee, Y. J.; Jang, S. G.; Kim, B. J. Light-Responsive, Shape-Switchable Block Copolymer Particles. *J. Am. Chem. Soc.* **2019**, *141* (38), 15348–15355.

(31) Mei, S.; Jin, Z. Mesoporous Block-Copolymer Nanospheres Prepared by Selective Swelling. *Small* **2013**, *9* (2), 322–329.

(32) Steinhaus, A.; Chakroun, R.; Müllner, M.; Nghiem, T.-L.; Hildebrandt, M.; Gröschel, A. H. Confinement Assembly of ABC Triblock Terpolymers for the High-Yield Synthesis of Janus Nanorings. *ACS Nano* **2019**, *13* (6), 6269–6278.

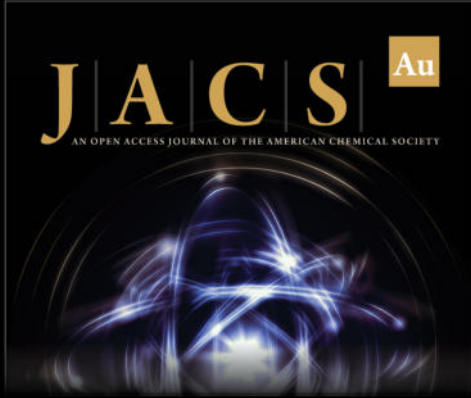
(33) Deng, R.; Liang, F.; Zhou, P.; Zhang, C.; Qu, X.; Wang, Q.; Li, J.; Zhu, J.; Yang, Z. Janus Nanodisc of Diblock Copolymers. *Adv. Mater.* **2014**, *26* (26), 4469–4472.

(34) Schmidt, B. V. K. J.; Wang, C. X.; Kraemer, S.; Connal, L. A.; Klinger, D. Highly functional ellipsoidal block copolymer nanoparticles: a generalized approach to nanostructured chemical ordering in phase separated colloidal particles. *Polym. Chem.* **2018**, *9* (13), 1638–1649.


(35) Seo, Y.; Woo, D.; Li, L.; Li, W.; Kim, J. K. Phase Behavior of PS-(PS-*b*-P2VP)₃ Miktoarm Star Copolymer. *Macromolecules* **2021**, *54* (17), 7822–7829.


(36) Tashiro, K.; Yoshioka, A. Molecular Mechanism of Solvent-Induced Crystallization of Syndiotactic Polystyrene Glass. 2. Detection of Enhanced Motion of the Amorphous Chains in the Induction Period of Crystallization. *Macromolecules* **2002**, *35* (2), 410–414.


(37) Ren, M.; Hou, Z.; Zheng, X.; Xu, J.; Zhu, J. Electrostatic Control of the Three-Dimensional Confined Assembly of Charged Block Copolymers in Emulsion Droplets. *Macromolecules* **2021**, *54* (12), 5728–5736.



JACS Au
AN OPEN ACCESS JOURNAL OF THE AMERICAN CHEMICAL SOCIETY

 Editor-in-Chief
Prof. Christopher W. Jones
Georgia Institute of Technology, USA

Open for Submissions 

pubs.acs.org/jacsau  ACS Publications
Most Trusted. Most Cited. Most Read.

Supporting Information

Solvent annealing of striped ellipsoidal block copolymer particles: Reversible control over lamellae asymmetry, aspect ratio and particle surface

Lucila Navarro¹, Andreas F. Thünemann² and Daniel Klinger^{1*}

¹ Institute of Pharmacy (Pharmaceutical Chemistry), Freie Universität Berlin, Königin-Luise Straße 2-4, 14195 Berlin, Germany

² Bundesanstalt für Materialforschung und -prüfung (BAM), Unter den Eichen 87, 12205 Berlin, Germany

*daniel.klinger@fu-berlin.de

Materials.

All chemical reagents were purchased from commercial sources and used without further purification: Cetyl trimethyl ammonium bromide (CTAB, Sigma Aldrich, $\geq 99\%$), toluene (Fisher, ACS grade), chloroform (Fisher, HPLC grade), iodine (ACROS Organics, pure). Poly (styrene-*block*-2-vinyl pyridine) polymer with a molecular weight of 102k-97 kDa was purchased from Polymer Source Inc. 16-hydroxy-N,N,N-triethylhexadecan-1-ammonium bromide (CTEAB-OH) was synthesized according to the literature.^{1, 2}

Methods

Transmission electron microscopy (TEM)

Before sample preparation, block copolymer particles were first purified by performing 3 cycles of centrifugation (6000 rpm, 5 min) and resuspension in Milli-Q water to remove the surfactants. TEM samples were prepared by applying a 10 μ L droplet of the purified particle solution on a carbon-coated copper grid (400 meshes, Quantifoil Micro Tools GmbH, Großlöbichau, Germany) for 45 s. The liquid was then removed by blotting with filter paper. The samples were allowed to dry in air overnight. The P2VP phase was stained by placing the samples on the TEM grids in an iodine chamber for 15 minutes. The measurements were performed in the TEM mode of a Hitachi Scanning Electron Microscope (SU8030, Hitachi High-Technologies Corporation, Tokyo, Japan) with a working voltage of 30.0 kV.

Small-angle X-ray scattering (SAXS)

Small-angle X-ray scattering (SAXS) measurements were performed using a modified Xeuss 2.0 instrument (Xenocs, Sassenage France). X-rays were generated from a microfocus X-ray tube with a copper target, followed by a multilayer optic to parallelize and monochromatize the X-ray beam to a wavelength of 0.154 nm. The instrument has a vacuum motorized detector (Eiger 1M, Dectris, Baden-Daettwil, Switzerland). The samples with a volume of 4 ml were probed within a flow-through cell under constant flow to avoid sedimentation. The sample cell was equipped with SiN windows. The resulting data were processed using the DAWN software package according to standardized procedures^{3,4}.

The simplest model we found for interpretation of the scattering profiles is that the scattering is given by an q^{-4} -scaling (Porod's law), two peak functions and a constant background b . This composite model is given by equation (1):

$$I(q) = a q^{-4} + \sum_{i=1}^2 I_{p,i}(q) + b \quad (1)$$

Exploration of the data reveals that neither Gaussian nor Lorentzian curve profiles provide satisfactory curve fits for both data sets. Therefore, we utilized a pseudo-Voit function for $I_{p,i}(q)$, which is a linear combination of a Gaussian and Lorentzian profile as equation (2):

$$I_{p,i}(q) = \frac{(1-\alpha_i)A_i}{\sigma_{G,i}\sqrt{2\pi}} \exp\left[-\frac{(q-q_i)^2}{2\sigma_{G,i}^2}\right] + \frac{\alpha_i A_i}{\pi} \left[\frac{\sigma_i}{(q-q_i)^2 + \sigma_i^2}\right] \quad (2)$$

Here α_i is the relative fraction of the Gaussian, A_i is the peak amplitude and q_i is the position of the peak maximum. The $\sigma_{G,i} = \sigma_i/\sqrt{2 \ln 2}$ is the width parameter of the Gaussian where σ_i is the width parameter of the Lorentzian. The width definition of the Gaussian $\sigma_{G,i}$ was chosen so that the full width at half maximum of the peak is $2\sigma_i$. The respective fitting parameters are shown in Table S1 for the pristine particles and the particles annealed with 200 wt% toluene.

Table S1. Fitting parameters for $I_{p,i}(q)$ according to equation (2) for SAXS scattering curves of pristine particles and particles annealed with 200 wt% toluene.

pristine particles		annealed particles (200 wt% toluene)	
variable	value	variable	value
V1_amplitude	18,6	V1_amplitude	47
dV1_amplitude	0	dV1_amplitude	0
V1_center	0,084	V1_center	0,06
dV1_center	0	dV1_center	0
V1_sigma	0,021	V1_sigma	0,02
dV1_sigma	0	dV1_sigma	0
V1_fraction	0	V1_fraction	0,3
dV1_fraction	0	dV1_fraction	0
V1_fwhm	0,042	V1_fwhm	0,04
dV1_fwhm	0	dV1_fwhm	0
V1_height	416	V1_height	997
dV1_height	0	dV1_height	0
V2_amplitude	0	V2_amplitude	10
dV2_amplitude	0	dV2_amplitude	0
V2_center	0,168	V2_center	0,12
dV2_center	0	dV2_center	0
V2_sigma	0,042	V2_sigma	0,03
dV2_sigma	0	dV2_sigma	0
V2_fraction	0	V2_fraction	0,3
dV2_fraction	0	dV2_fraction	0
V2_fwhm	0,084	V2_fwhm	0,06
dV2_fwhm	0	dV2_fwhm	0
V2_height	0	V2_height	141
dV2_height	0	dV2_height	0
a	0,00188	V3_amplitude	0
da	0,0000551	dV3_amplitude	0
V3_amplitude	1,45	V3_center	0,24
dV3_amplitude	0	dV3_center	0
V3_center	0,252	V3_sigma	0,05
dV3_center	0	dV3_sigma	0
V3_sigma	0,063	V3_fraction	0,3
dV3_sigma	0	dV3_fraction	0
V3_fraction	0	V3_fwhm	0,1
dV3_fraction	0	dV3_fwhm	0
bkg	0,02	V3_height	0
dbkg	0	dV3_height	0
d	75	a	0,00704
lc	300	da	0,000159
qmin	0,012	bkg	0,005
dmax	260	dbkg	0

Preparation of striped ellipsoidal particles

PS-*b*-P2VP striped ellipsoidal particles were prepared by the emulsion-solvent evaporation method, as previously reported.¹ Two aqueous stock solutions of CTEAB-OH (1 mg/mL) and CTAB (1 mg/mL) were prepared in Milli-Q water with slight heating to assure the complete dissolution of the surfactants. Portions of these solutions (70 wt% of CTEAB-OH solution and 30 wt% of CTAB solution) were mixed to give 5 g of a mixed surfactant solution. To this mixture, 5 g of Milli-Q water were added to obtain a total of 10 g continuous phase with an overall surfactant concentration of 0.05 wt%. This exact surfactant composition was used in order to achieve surface neutrality and obtain a lamellar morphology with both domains orientated perpendicular to the particle interface.^{1, 2} The polymer solution was prepared in chloroform with a concentration of 1 wt% of PS-*b*-P2VP. 1.5 g was added to the surfactant solution in a screw cap vial. Emulsification was performed by vortexing and sonication in an ultrasound bath. Afterwards, chloroform was let to evaporate by stirring the open vials at 32 °C for 48 h. Finally, the resulting particle suspensions were wash three times by cycles of centrifugation and resuspension in Milli-Q water.

Selective solvent swelling and annealing

A certain volume of un-washed aqueous suspension of the particles (1.5 mg/mL in the corresponding surfactant solution) was transferred into a glass reaction vial and a specific amount of toluene was added via micropipette. The vial was sealed and the solution was emulsified by briefly using vortex and sonication in an ultrasound bath (5 sec). The particles were left to swell by stirring for 14 h at room temperature. Finally, toluene was evaporated under different conditions (see Table S1 and Figures S7).

Surfactant variation during annealing procedure

1 mL of pristine particle suspension (1.5 mg/mL) was purified by 4 cycles of centrifugation and re-suspension in Milli-Q water. During the last cycle, instead of Milli-Q water, a mixed surfactant solution of CTEAB-OH and CTAB was used for resuspension. Here, the composition of the surfactant mixture was varied to give different mass fractions of CTEAB-OH (Table S2). The suspension was transferred to a 1.5 mL glass vial and different amounts of toluene were added via micropipette. The vials were sealed and the mixture was emulsified by briefly using vortex and sonication. The particles were left to swell by stirring for 14 h at room temperature. Afterwards the vial was opened to air and the solvent was left to evaporate at 32 °C for 48 h under stirring.

Supporting data and figures

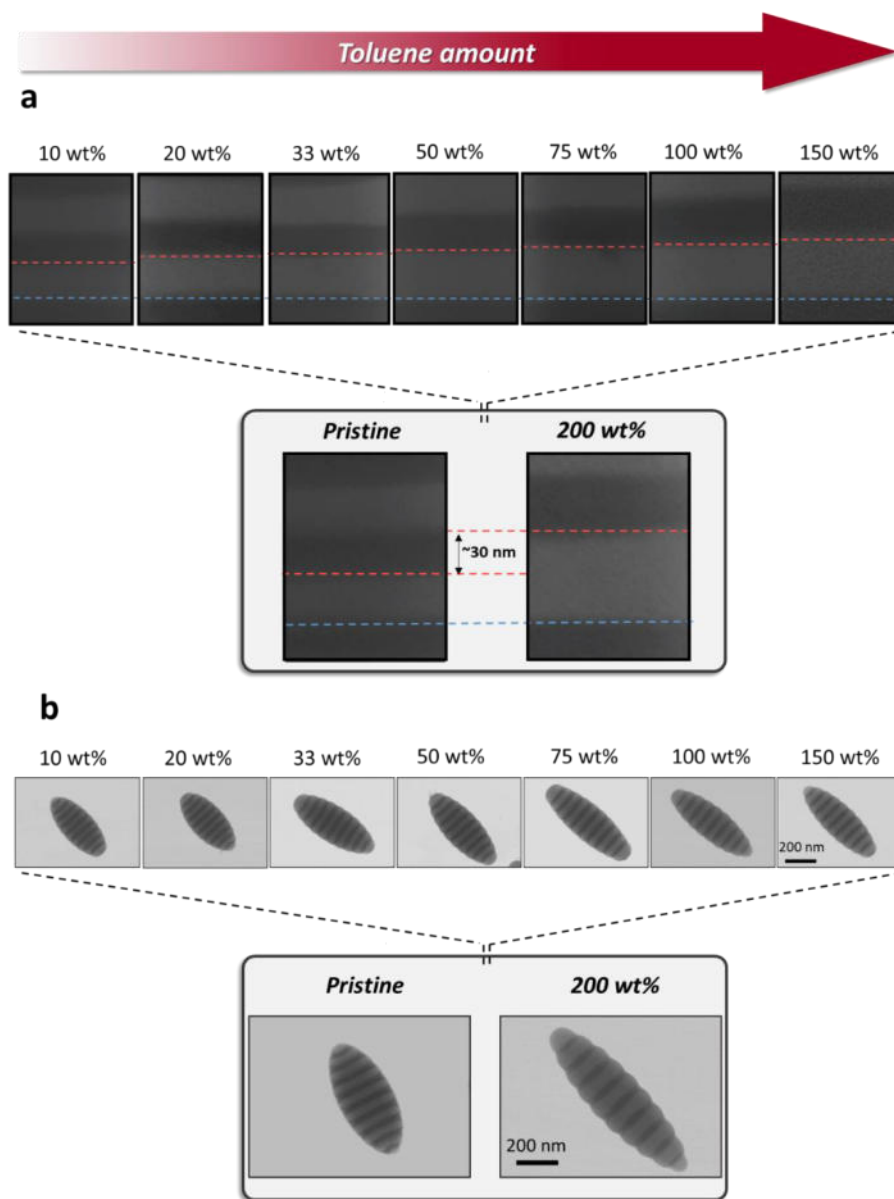


Figure S1. Annealing of PS-*b*-P2VP particles with different amounts of toluene (wt% w.r.t. particle mass) enables tuning the PS lamellae thickness. This is translated into particle elongation. (a) TEM pictures of the middle section of ellipsoidal particles after toluene annealing. A stepwise and selective increment of the PS lamellae thickness can be observed with each increment of toluene. (b) TEM pictures of annealed particles show an increase of particle length while the width remains constant. As result, the aspect ratio increases with the amount of toluene during annealing.

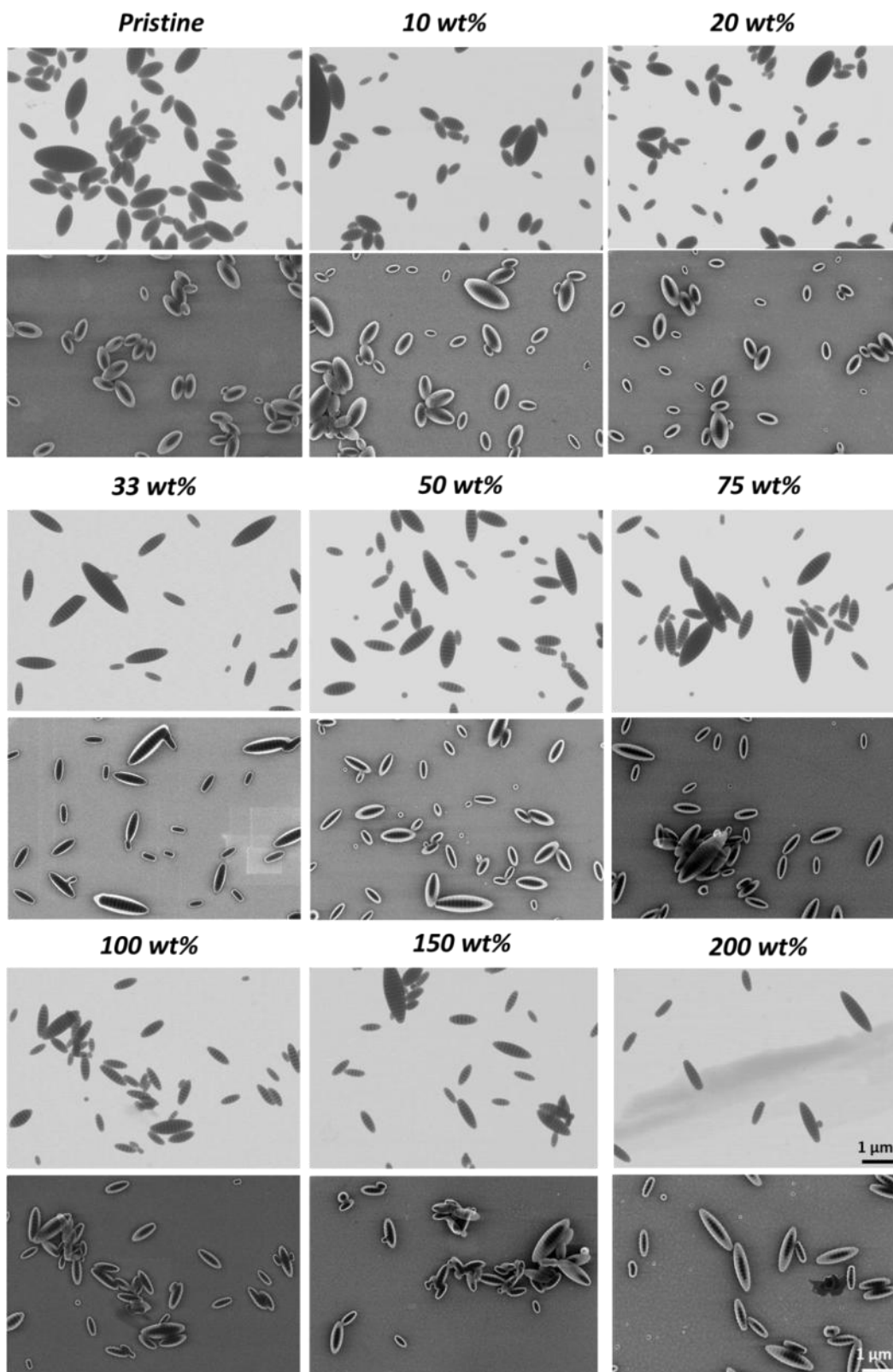


Figure S2. Selection of TEM and SEM images showing multiple particles per sample for each annealing condition.

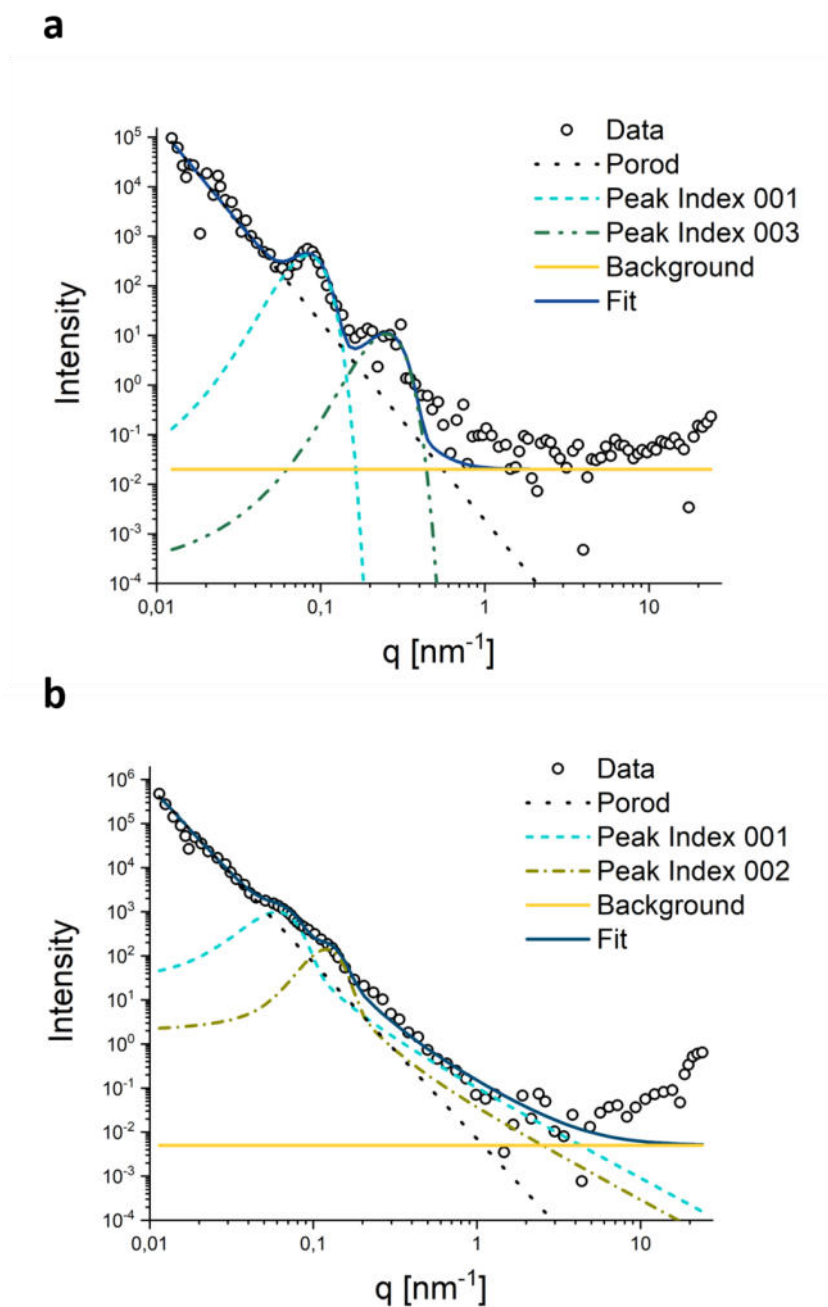


Figure S3. Small angle x-ray analysis of particles before and after annealing with toluene. Scattering pattern of (a) pristine particles and (b) particles annealed with 200 wt% of toluene. Both Figures include the actual data and the respective fits with the individual contributions as described earlier. In each sample, clear peaks are visible that correspond to reflections (001), (002) or (003). However, not all reflections are observed in each sample. The (002) is absent in Figure S3 a and (003) is absent in Figure S3 b.

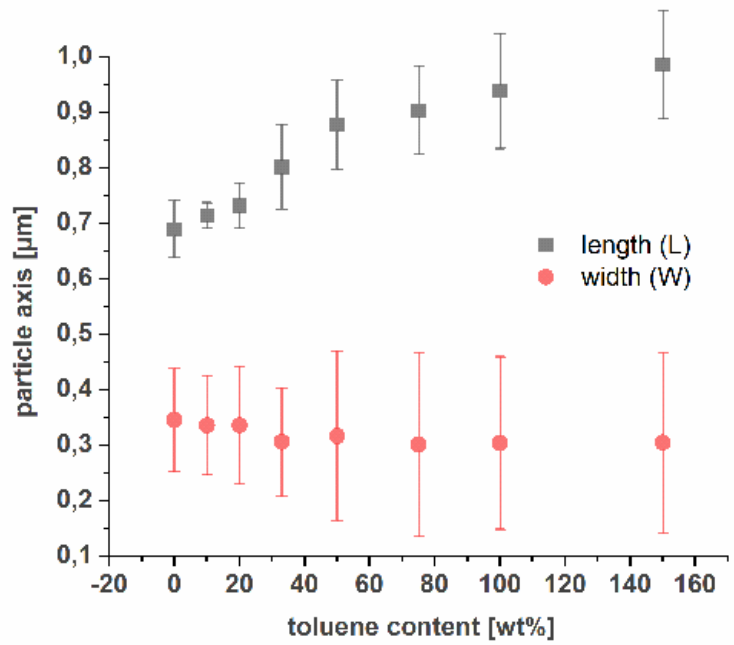


Figure S4. Length (L) and width (W) for particles with 10 PS lamellae after annealing with varying toluene contents. It is shown that particle length increases with toluene content whereas particle width remains constant. Each data point represents the average of at least 20 particles measured by analysis of TEM images. Error bars represent the standard deviation.

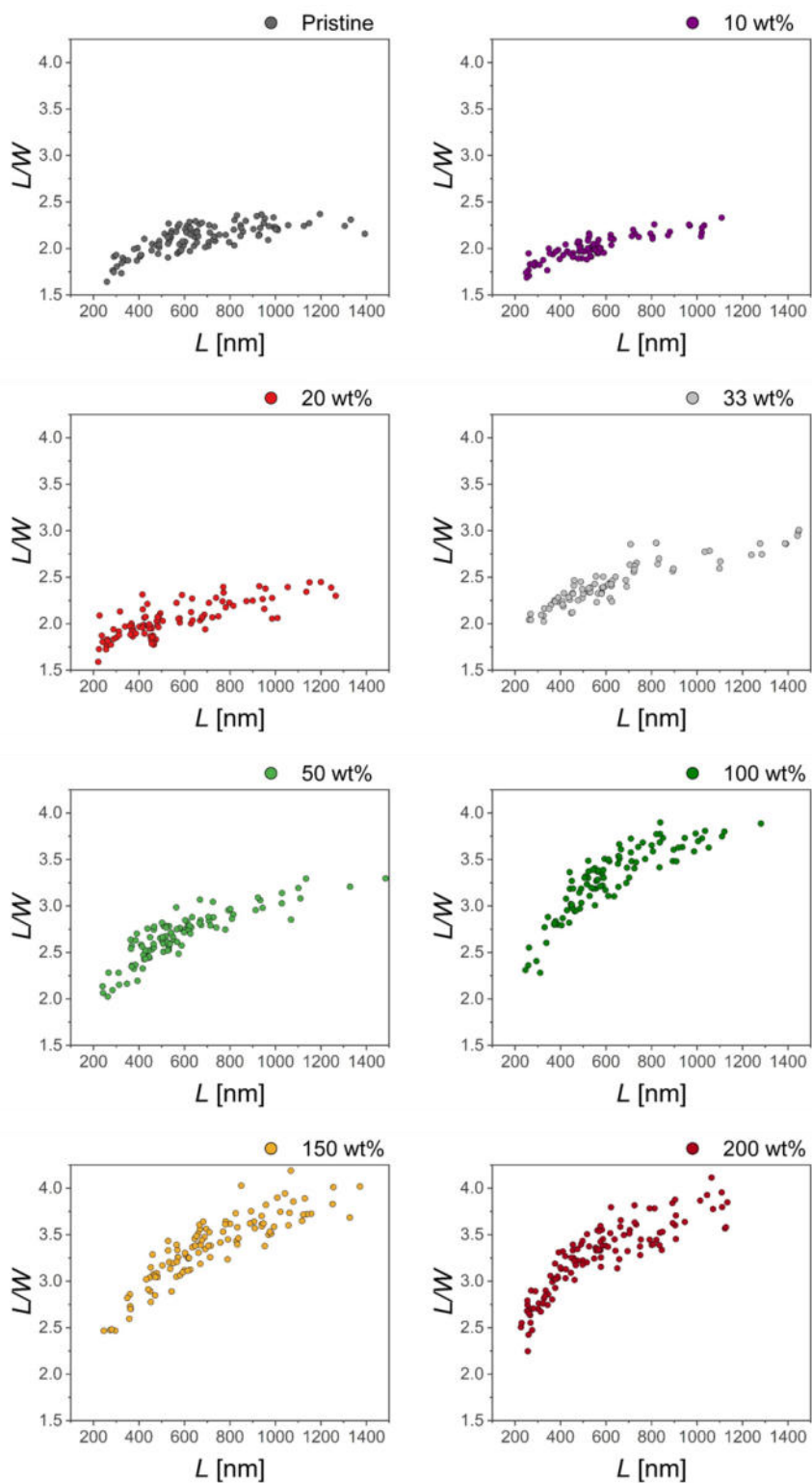


Figure S5. Influence of the toluene amount on the particle aspect ratio ($AR = L/W$) of striped ellipsoidal particles during the swelling/annealing process. Plots of the AR distribution *versus* the particle length (L). The aspect ratio is defined as ratio between particle length (L) and width (W).

Table S2. Evaluated parameters during the toluene annealing procedure. Influence of: swelling temperature (blue section), swelling time (red section), evaporation conditions (green section).

Toluene fraction [wt%]	Swelling temperature [°C]	Swelling time [h]	Solvent evaporation conditions	Reference to Figure
100	RT	14	Stirring, 32°C, 48h	Fig S5
100	70	14	Stirring, 32°C, 48h	Fig S5
100	RT	0.33	Stirring, 32°C, 48h	Fig S6
100	RT	2	Stirring, 32°C, 48h	Fig S6
100	RT	6	Stirring, 32°C, 48h	Fig S6
100	RT	14	Stirring, 32°C, 48h	Fig S6
100	RT	14	Stirring, 32°C, 48h	Fig S7
100	RT	14	Stirring, 70°C, 48h	Fig S7
100	RT	14	70°C in vacuum, 6h	Fig S7

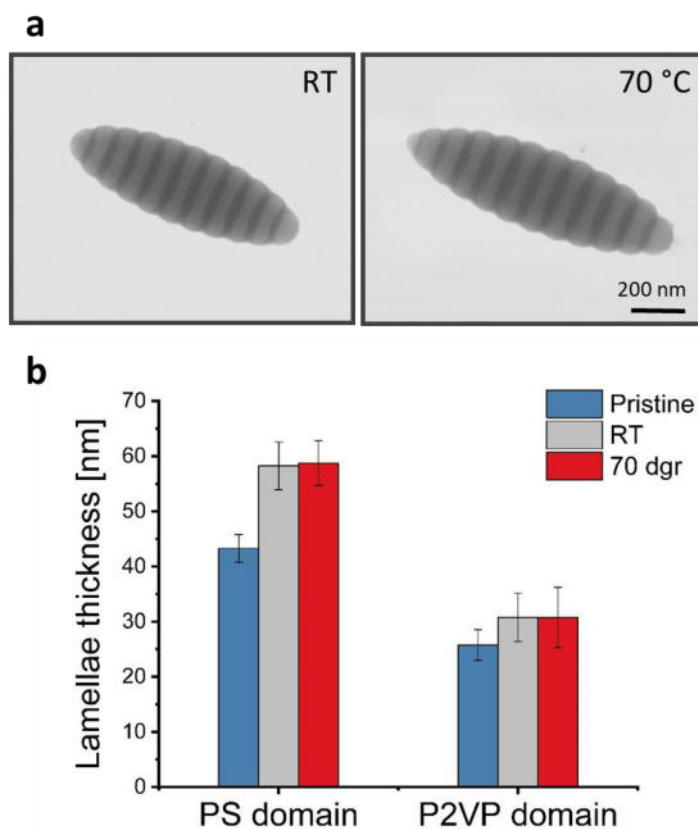


Figure S6. Examining the effect of toluene swelling temperature on the PS-*b*-P2VP particle morphology and lamellae thickness. Particles were first swollen with 100 wt% of toluene at either RT or 70 °C for 14 hrs. Afterwards, toluene was evaporated at 32°C over 48 hrs. (a) TEM pictures of particles swollen with toluene at RT (left) and 70 °C (right). (b) PS and P2VP lamellae thickness corresponding to the different swelling temperatures. While clear differences to the non-annealed pristine particles are visible, both annealed samples show the same lamellae thickness and particle shape. This suggests that the swelling temperature (in the investigated temperature range) has no impact on the final morphology of the particles.

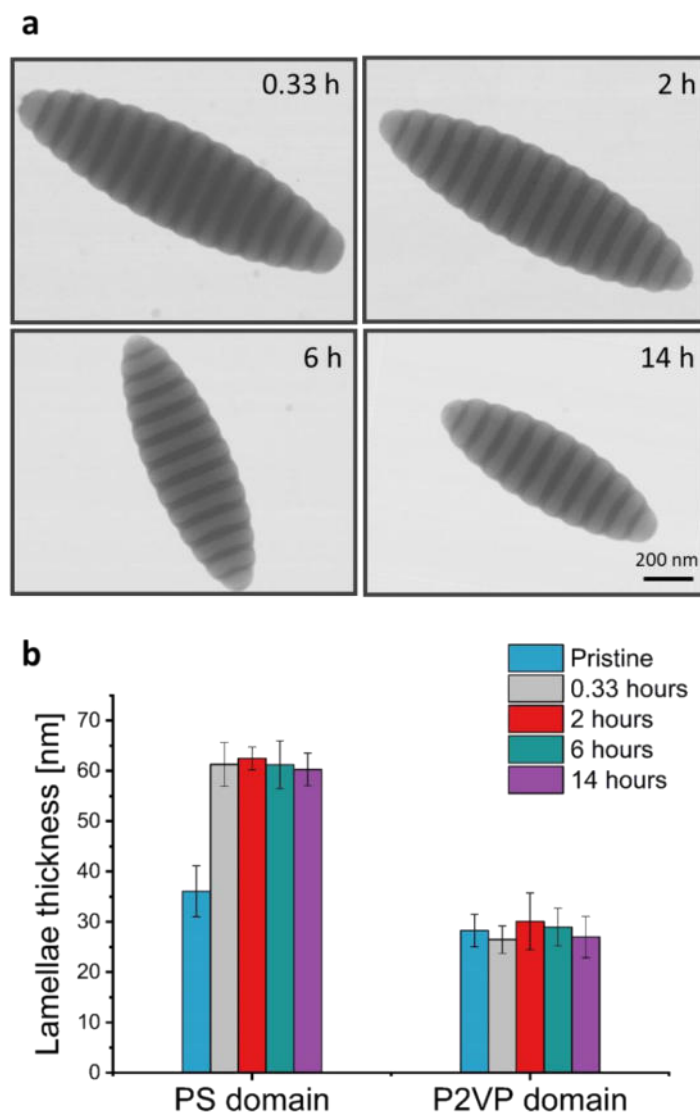


Figure S7. Evaluating the effect of toluene swelling time on the PS-*b*-P2VP particle morphology and lamellae thickness. Particles were first swollen with 100 wt% of toluene at RT for different times (0.33, 2, 6 and 14 h). Afterwards, the toluene was evaporated at 32°C over 48 hrs. (a) TEM pictures of particles after first swelling with toluene for 0.33, 2, 6 and 14 h and subsequent toluene evaporation. (b) PS and P2VP lamellae thickness corresponding to the different swelling times during the annealing process. While clear differences to the non-annealed pristine particles are visible, all annealed particles showed the same lamellae thickness and particle shape, thus indicating that swelling time (in the tested time range) has no impact on the final morphology.

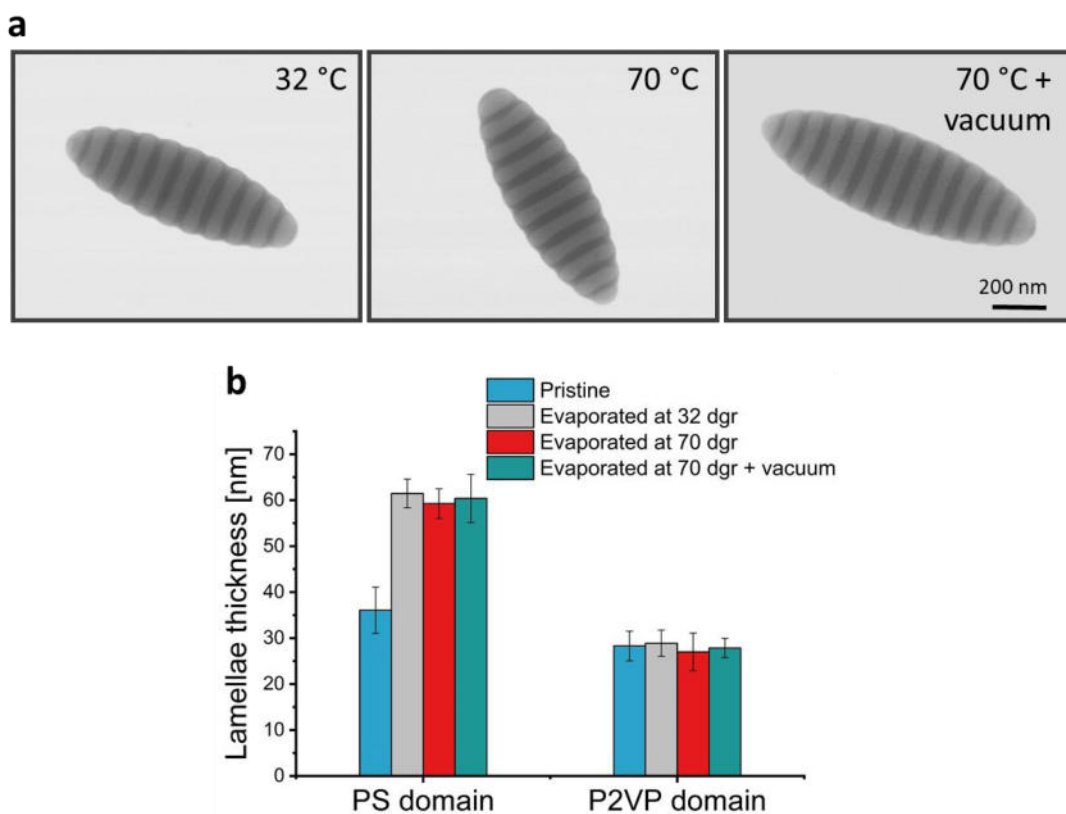


Figure S8. Investigating the effect of toluene evaporation rate on the PS-*b*-P2VP particle morphology and lamellae thickness. Particles were first swollen with 100 wt% of toluene at RT for 14 h. Afterwards, the toluene was evaporated either at 32°C or at 70°C over 48 hrs under stirring. Alternatively, toluene evaporation was performed at 70 °C in vacuo using a rotary evaporator. (a) TEM pictures of particles swollen with toluene and solvent evaporation at 32 °C, 70 °C and 70 °C in vacuo using a rotary evaporator. (b) PS and P2VP lamellae thickness corresponding to the different evaporation conditions. While clear differences to the non-annealed pristine particles are visible, all annealed particles showed the same lamellae thickness and particle shape, thus indicating that evaporation rate (in the tested range of conditions) has no impact on the final morphology.

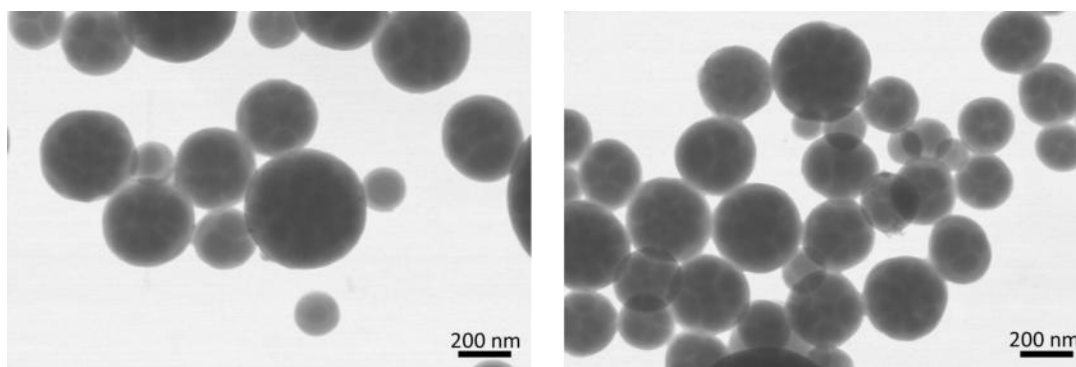


Figure S9. TEM pictures of particles annealed with 250 wt% of toluene. The striped ellipsoidal particles have transformed into spherical particles with multiple internal P2VP domains.

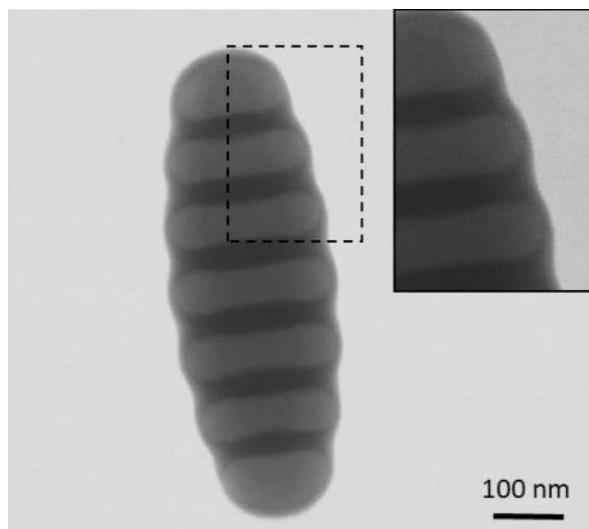


Figure S10. Detailed TEM image of the surface of a particle annealed with 100 wt% of toluene. The addition of toluene increases the thickness of the PS domains and induces partial migration of P2VP to the particle surface. This particle restructuring is assumed to be the result of an increased mobility of both BCP segments. Toluene can selectively swell the PS domains already in small quantities. In higher concentrations it is assumed to act as plasticizer for the P2VP domains, too. This enables increase in PS domain thickness due to chain stretching and migration of P2VP to the particle surface due to an enhanced interaction with the aqueous phase.

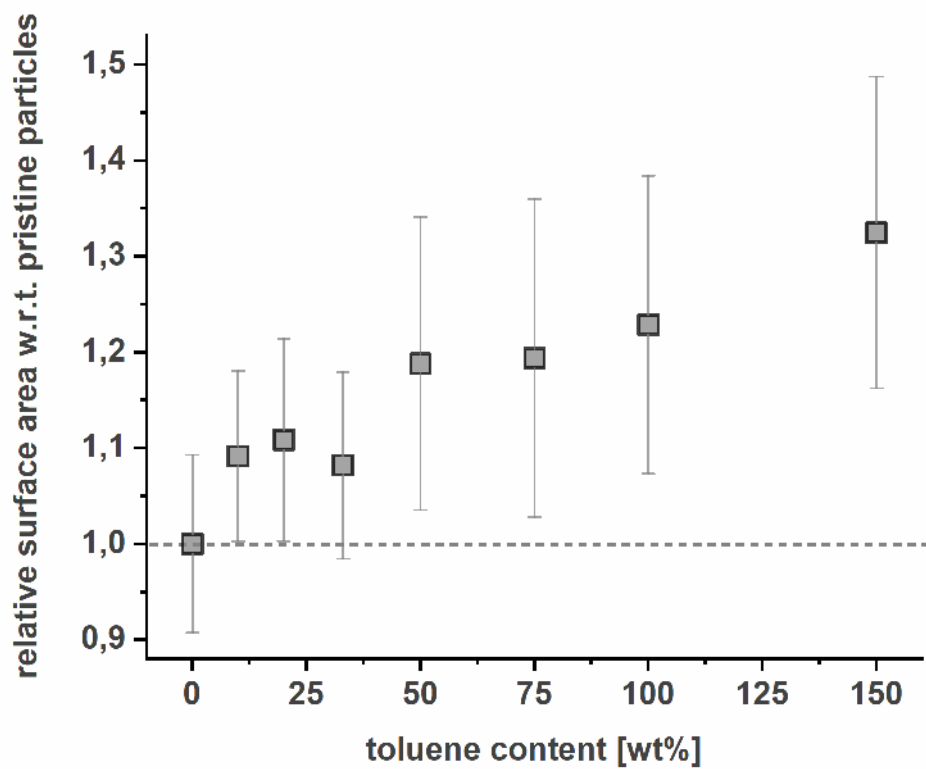


Figure S11. Particle surface area (relative to pristine particles) increases with toluene content upon annealing. This is the result of an increasing PS domain size.

Table S3. Examined parameters to study the effect of surfactants on the particle surface morphology during annealing with toluene. Varying the toluene amount (20, 50, 150, and 200 wt%) for different mixtures of PS-selective CTAB and P2VP-selective CTEAB-OH surfactants.

Toluene fraction [wt%]	Surfactant fraction [wt%]		Interface morphology
	CTEAB-OH	CTAB	
20	0	100	Surface neutrality
50	0	100	Surface neutrality
150	0	100	Mix morphology
200	0	100	PS domain migration
20	30	70	Surface neutrality
50	30	70	Surface neutrality
150	30	70	Surface neutrality
200	30	70	Surface neutrality
150	65	35	Partial P2VP domain migration
150	75	25	Partial P2VP domain migration
20	100	0	P2VP domain migration
50	100	0	P2VP domain migration
150	100	0	P2VP domain migration
200	100	0	P2VP domain migration

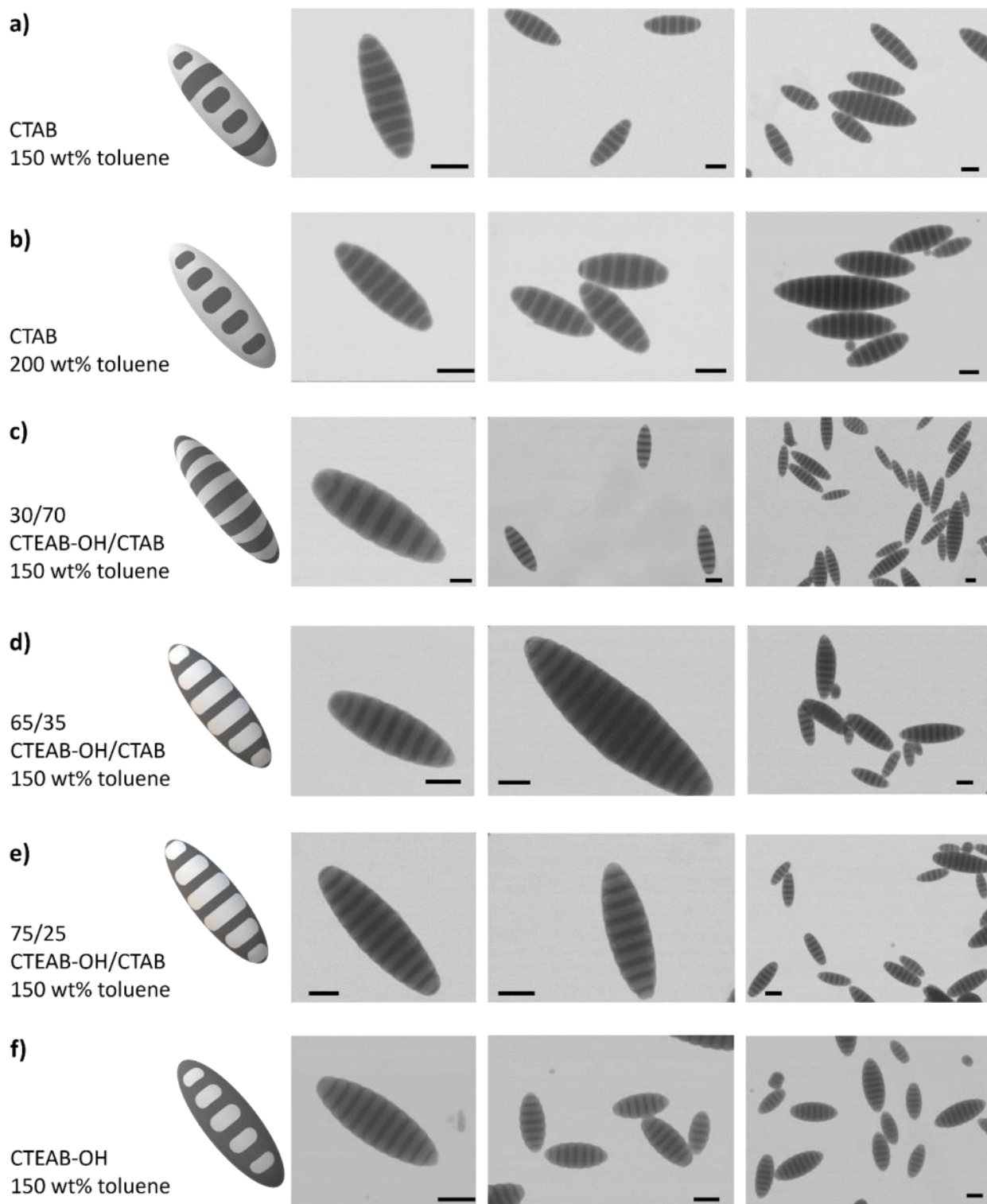


Figure S12. TEM images of different particle surface morphologies obtained by varying surfactant mixture and toluene amount during annealing. (a) Using only CTAB as surfactant and 150 wt% of toluene, an intermediate morphology is observed. At the particle surface, some areas are wetted

equally by both blocks and other parts show PS migration to the surface. (b) Using only CTAB as surfactant but increasing the toluene amount to 200 wt%, complete PS migration to the surface is observed. (c) Using a 30/70 wt% mixture of CTEAB-OH/CTAB surfactants and 150 wt% of toluene, neutral wetting of the particle surface and highly elongated particles are obtained. For mixtures with CTEAB-OH/CTAB ratios of 65/35 wt% (d) and 75/25 wt% (e), the P2VP domains are starting to partially engulf the PS domains. (f) Using only CTEAB-OH, migration of P2VP segments to the surface is observed for annealing with 20-200 wt% toluene (specific particles depicted in image (f) correspond to 150 wt% toluene addition). Scale bar showed in every picture correspond to a value of 200 nm.

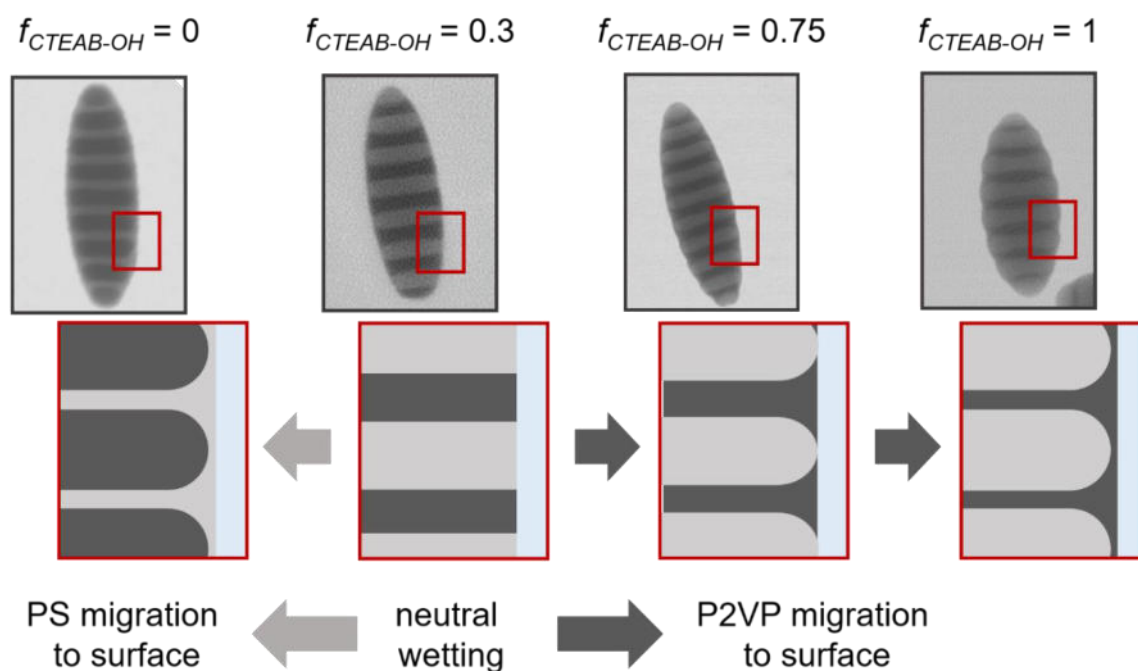


Figure S13. Particle annealing with varying surfatcant mixtures ($f_{CTEAB-OH}$) and constant toluene content of 150 wt% allows tuning the particle surface morphology. At $f_{CTEAB-OH} = 0.3$, neutral wetting of the interface is observed. For other CTEAB-OH contents, a partial rearrangement of the BCP at the particle/water interface is observed. For excess CTEAB-OH ($f_{CTEAB-OH} > 0.3$),

preferential interaction of P2VP with CTEAB-OH causes a partial engulfing of the PS domains by P2VP. This is complete for using pure CTEAB-OH ($f_{CTEAB-OH} = 1$). For excess CTAB ($f_{CTEAB-OH} < 0.3$) preferential interaction of PS with CTAB causes a (partial) engulfing of the P2VP domains by PS.

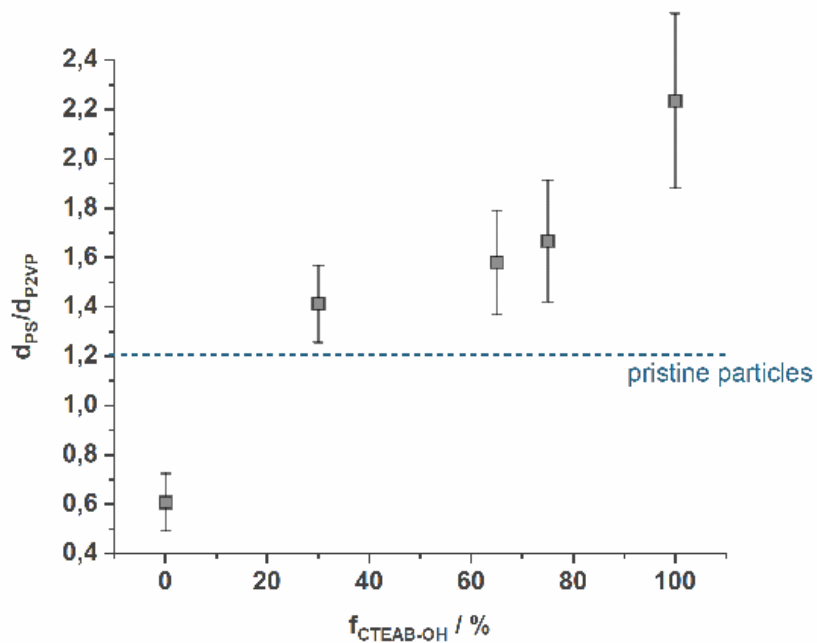


Figure S14. Lamellar asymmetry ratio is described by the thickness ratio between PS and P2VP lamellae (d_{PS}/d_{P2VP}). For a constant amount of toluene (150 wt%) during annealing, the lamellar asymmetry depends on the surfactant ratio $f_{CTEAB-OH}$.

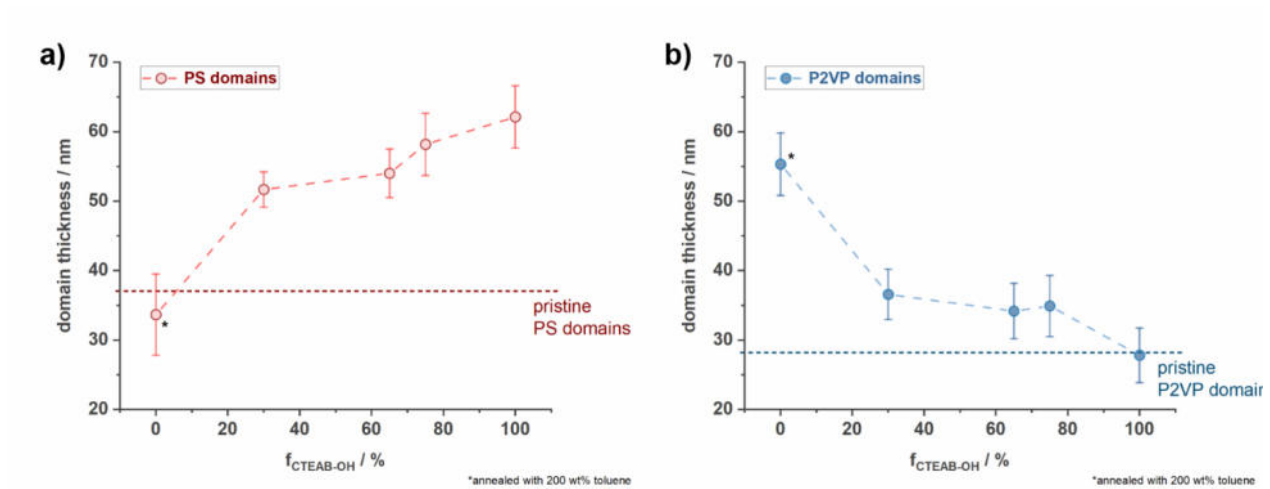


Figure S15. For annealing with a constant amount of toluene (150 wt%), the lamellar thickness of (a) PS and (b) P2VP domains depends on the surfactant composition ($f_{\text{CTEAB-OH}}$). An increase of block-selective surfactant causes migration of the respective block to the surface. This stabilizes an increased surface area of the other block. For example, for increasing contents of P2VP-selective CTEAB-OH, the PS domain size increases. Simultaneously, the P2VP domain size decreases to the size of the P2VP domains in the pristine particles.

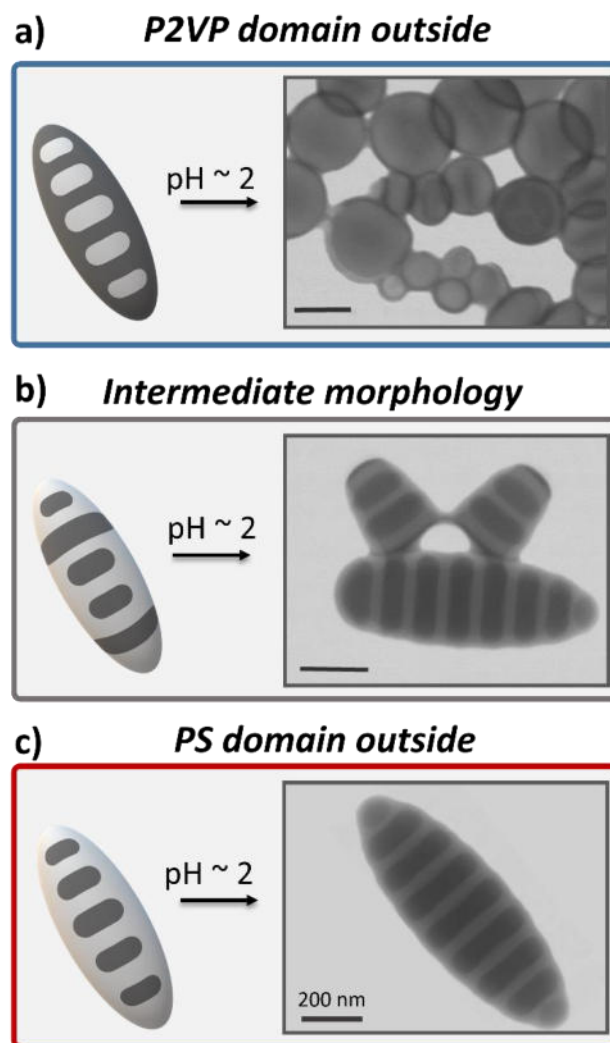


Figure S16. Examining the effect of acidic pH (pH 2) on the different particle morphologies. a) For particles annealed in a CTEAB-OH solution, P2VP covers the entire particle surface. Decreasing the pH of this suspension causes protonation of the pyridine group and the disassembly of the particles into discrete PS disks with a corona of solubilized P2VP chains. b) For annealing with 150 wt% of toluene in a CTAB solution, an intermediate mixed particle morphology is obtained. Acidification results in the protonation of the pyridine groups from the P2VP domains that are exposed to the interface, thus demonstrating the mixed morphology. c) Using 200 wt% of toluene for annealing in a CTAB solution, migration of PS covers the entire particle surface. This PS shell acts as a protective layer against disassembly of the particles at low pH.

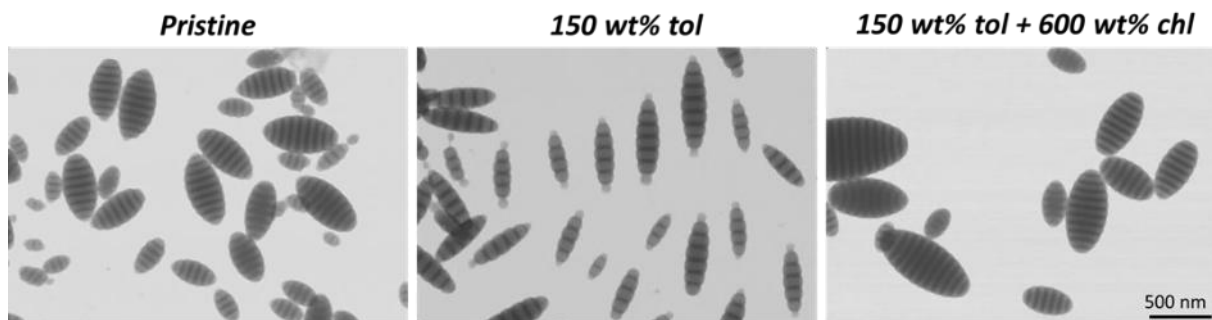


Figure S17. TEM images of non-annealed pristine particles, particles annealed with 150 wt% of toluene and particles that were re-swollen with 600 wt% of chloroform after the first annealing step. The shown overviews of the samples demonstrate that selective annealing with toluene tends to expand the PS domains and that re-swelling with chloroform as unselective solvent restores the original shape and morphology of the particles. The reversibility of the system is suggested to stem from due an equal mobilization of both, PS and P2VP, segments.

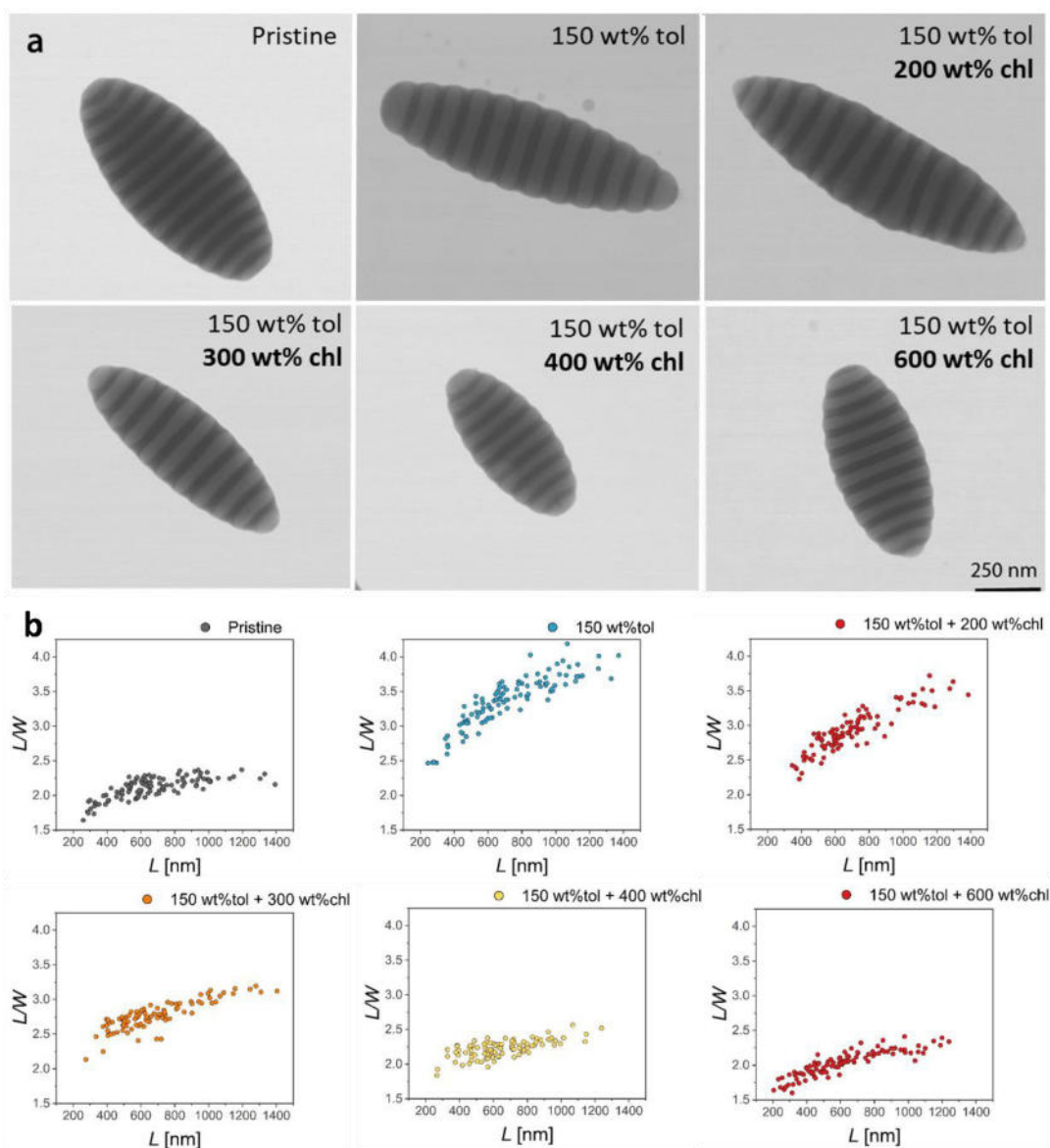


Figure S18. For toluene-annealed particles, a second annealing step with chloroform as non-selective solvent restores the original shape and morphology. (a) TEM images demonstrate the dependence of this process on the amount of chloroform. The addition of 200 wt% of chloroform generates lamellae of un-even thickness. Increasing the amount of chloroform to 300 and 400 wt% significantly decreases the lamellae asymmetry until a full return to original shape (given by the aspect ratio) and morphology (given by the lamella thickness) is achieved with 600 wt% of chloroform. (b) Plots of aspect ratio vs. particle length for the different chloroform treatments show that pristine particle shape and morphology is approached with increasing amounts of toluene.

References

1. Klinger, D.; Wang, C. X.; Connal, L. A.; Audus, D. J.; Jang, S. G.; Kraemer, S.; Killops, K. L.; Fredrickson, G. H.; Kramer, E. J.; Hawker, C. J. A Facile Synthesis of Dynamic, Shape-Changing Polymer Particles. *Angew. Chem. Int. Ed.* **2014**, 53 (27), 7018-7022 DOI: <https://doi.org/10.1002/anie.201400183>.
2. Schmidt, B. V. K. J.; Wang, C. X.; Kraemer, S.; Connal, L. A.; Klinger, D. Highly functional ellipsoidal block copolymer nanoparticles: a generalized approach to nanostructured chemical ordering in phase separated colloidal particles. *Polym. Chem.* **2018**, 9 (13), 1638-1649 DOI: 10.1039/C7PY01817G.
3. Filik, J.; Ashton, A. W.; Chang, P. C. Y.; Chater, P. A.; Day, S. J.; Drakopoulos, M.; Gerring, M. W.; Hart, M. L.; Magdysyuk, O. V.; Michalik, S.; Smith, A.; Tang, C. C.; Terrill, N. J.; Wharmby, M. T.; Wilhelm, H. Processing two-dimensional X-ray diffraction and small-angle scattering data in DAWN 2. *Journal of Applied Crystallography* **2017**, 50 (3), 959-966 DOI: doi:10.1107/S1600576717004708.
4. Pauw, B. R.; Smith, A. J.; Snow, T.; Terrill, N. J.; Thünemann, A. F. The modular small-angle X-ray scattering data correction sequence. *Journal of Applied Crystallography* **2017**, 50 (6), 1800-1811 DOI: doi:10.1107/S1600576717015096.